The Y–Mg–Co ternary system: alloys synthesis, phase diagram at 500 °C and crystal structure of the new compounds

V.V. Shtender, V.V. Pavlyuk, O.Ya Zelinska, W. Nitek, V. Paul-Boncour, G.S. Dmytriv, W. Łasocha, I.Yu Zavaliy

$TbMgNi_{4-x}Co_x$–$(H,D)_2$ System: I. Synthesis, Hydrogenation properties, Crystal and Electronic structures

V.V. Shtender[1,2,*], V. Paul-Boncour[1], R.V. Denys[3], J.-C. Crivello[1], I.Yu. Zavaliy[2]

[1]*Université Paris-Est Creteil, CNRS, ICMPE, UMR 7182, F-94320 Thiais, France*

[2]*Karpenko Physico-Mechanical Institute, NAS of Ukraine, 5 Naukova St., 79060 Lviv, Ukraine*

[3]*HYSTORSYS AS, P.O. Box 45, Kjeller NO-2027, Norway*

*Corresponding Author

*E-mail: shtender@glvt-cnrs.fr

Abstract

Series of cubic $TbMgNi_{4-x}Co_x$ (x = 0–4) pseudo binary compounds have been synthesized either by solid state reaction or mechanical alloying with further annealing treatment. Their hydrogenation properties have been studied by Pressure-Composition-Temperature (*PCT*) measurements, showing the formation of α-, β- and γ-hydrides. The Co for Ni substitution yields a lowering of the equilibrium pressure and an increase of hydrogen capacity. An improvement of the kinetic of hydrogen absorption was observed for increasing Co content. The β-$TbMgNi_{4-x}Co_xH_{\sim 4}$ (x = 0–3) hydrides show an orthorhombic distortion ($Pmn2_1$ space group) whereas β-$TbMgCo_4H_{3.3}$ hydride crystallizes in a monoclinic structure (Pm space group) derived from the orthorhombic structure. Sensitivity of the formation of the β-$TbMgCo_4H_{3.3}$ hydride to the temperature has been observed in *PCT* curves: it exists below 50 °C. γ-$TbMgNi_{4-x}Co_xH_y$ (x = 2–4, y > 5) hydrides preserve the parent cubic structure (F-43m space group) with an hydrogen induced volume expansion of 17.9–22.3 %. The deuterium for hydrogen substitution in $TbMgNiCo_3$–$(H,D)_2$ system prevents fast desorption at room temperature and ambient pressure The positions of deuterium atoms in the γ-$TbMgCo_4D_6$ deuteride were determined by neutron powder diffraction. Two types of interstitial sites were found occupied: 87 % of deuterium atoms (D1 site) are located inside Tb_2MgCo_2 octahedra and the remaining 13 % (D2 site) are inside Co_4 tetrahedra. The increase of Co content allows to improve the thermodynamic stability of $TbMgNi_{4-x}Co_x$ hydrides as demonstrated by the lowering of the desorption plateau pressure, the increase of the desorption temperature and of the enthalpy of formation versus Co content. This last experimental result is confirmed by first principles calculations where electronic structures of intermetallic compounds and their cubic $TbMgNi_{4-x}Co_xH_6$ hydrides are compared for x = 0, 2 and 4.

1. Introduction

Magnesium metal is one of the most attractive material for hydrogen storage with high hydrogen capacity (7.6 wt.%). However, due to some drawbacks as low kinetic and high hydride stability, its use as a medium for energy storage and transportation is limited. To improve both thermodynamic and kinetic properties, Mg-based binary and ternary intermetallic compounds have been extensively investigated[1-4]. Considerable research has been made on magnesium based composite materials, which have improved sorption-desorption characteristics[5-8].

The *R*–Mg–*T* (*R* = rare earth, *T* = Ni, Co, Cu) ternary alloys have attracted interest as hydrogen absorbing materials and particularly as effective negative electrodes for Ni–*M*H batteries. Mg-rich ternary compounds are of practical interest because their hydrogen capacity can reach 5.5 wt.%[2,4]. Moreover, Mg-rich alloys, containing more than 50 wt.% of Mg, decompose under hydrogenation into MgH_2, binary rare-earth hydrides (e.g., RH_x) and ternary magnesium transition-metal hydrides (e.g., Mg_2NiH_4)[4]. Nevertheless, these alloys have very interesting hydrolysis properties useful for hydrogen gas recovery[9]. At the same time, *R*-rich compounds can absorb hydrogen up to 2 wt.% and form crystalline or partially amorphous hydrides, but they decompose during desorption[10-13]. Finally, ternary or pseudo-binary Mg-containing compounds from the *T*-rich region can reversibly absorb hydrogen from the gas phase or electrochemically (~1.6 wt.%)[2]. For example, it is shown that the partial *R* substitution by Mg enhances hydrogen absorption properties of the binary RNi_2, RNi_3, R_2Ni_7 and R_5Ni_{19} compounds[1]. Compared to binary R_xNi_y phases, Mg-containing alloys ($R_{x-z}Mg_zNi_y$) have higher resistance against hydrogenation induced amorphization and thus form crystalline hydrides[14-16]. Rare earth–magnesium-based alloys played increasing roles in the solid-state hydrogen storage field.

Since Oesterreicher *et al.*[17] firstly studied $LaMgNi_4$ compound with $MgCu_2$/$SnMgCu_4$ structure type, many studies have been performed on the hydrogenation properties of the $RMgNi_4$ compounds (preferably with *R* = light rare earth)[1,4,18]. Our group has systematically investigated $RMgNi_{4-x}Co_x$ compounds for *R*= Ce[19], Y[20], Nd[21], La[22] and Pr[23]], where a 50 % increase of the hydrogen capacity was found upon Co for Ni substitution.

In this work, we have synthetized $TbMgNi_{4-x}Co_x$ alloys to show the influence of Tb as a heavy rare earth on the hydrogenation properties and crystal structure of the hydrides. The results obtained for these compounds are compared with those obtained for light rare earth.

In addition, first principles calculations were performed in the frame of electronic density functional theory (DFT) to analyze the modification of the electronic structures of $TbMgNi_{4-x}Co_x$ compounds upon hydrogen insertion and compare their phase stability with the experimental results.

2. Experimental methods

Starting materials for preparation of $TbMgNi_{4-x}Co_x$ (x = 0–4) intermetallic compounds (IMC) were ingots of Tb, Ni and Co (all with purity ≥ 99.9 %), and Mg powder (325 mesh, 99.8 %). In the first step, $TbNi_{4-x}Co_x$ (x = 0–4) alloy precursors were prepared by arc melting in purified argon atmosphere. The as-cast $TbNi_{4-x}Co_x$ buttons were ground in an agate mortar and then mixed with Mg powder in certain proportions. Mg was added with 3 wt.% excess in order to compensate for its evaporation loss at high temperatures. The powder mixtures were pressed into pellets, placed into tantalum containers, which were further loaded into a stainless-steel autoclave and sealed under Ar atmosphere. Alloys further denoted as No. 7 and No. 9 have been ball milled for 8 h in Ar atmosphere and placed into tantalum container without compressing. Then, several attempts have been made to prepare single phase alloys. All aspects of the heat treatment are summarized in Table 1. Structural analysis of the samples was carried out by X-ray powder diffraction (XRD) using Bruker D8 diffractometer (Cu-Kα radiation).

Electron Probe Micro Analysis (EPMA) has been performed for selected samples using SX 100 CAMECA with dispersion analysis of wavelength (WDS) to study the microstructures and elemental

compositions of the alloys. Pieces of the samples were placed in an aluminum holder, filled by Wood's alloys and then optically polished for analysis. The experimentally observed compositions were all within ±0.1 at. %.

Table 1. Conditions of synthesis and results of XRD analysis of $TbMgNi_{4-x}Co_x$ (x = 0–4) alloys.

No.	Alloy	Heat treatment	Cell parameter a (Å)	Composition according to Rietveld refinements	Phase analysis
1	$TbMgNi_4$	Slowly heated to 800 °C, then cooled to 500 °C and annealed at this temperature for ~250 h, quenched in cold water	7.0205(1)	$TbMgNi_4$	~99 % $TbMgNi_4$ + 1 % Tb_2Co_7
2	$TbMgNi_3Co$		7.0333(1)	$TbMgNi_3Co$	100 % $TbMgNi_3Co$
3	$TbMgNi_2Co_2$		7.0452(1)	$Tb_{0.87}Mg_{1.13}Ni_2Co_2$	93 % $TbMgNi_2Co_2$ + 7 % $TbCo_5$
4	$TbMgNi_2Co_2$		7.0441(3)	$Tb_{1.03}Mg_{0.97}Ni_2Co_2$	94 % $TbMgNi_2Co_2$ + 6 % $TbCo_5$
5	$TbMgNi_2Co_2$		7.0440(1)	$Tb_{1.03}Mg_{0.97}Ni_2Co_2$	91 % $TbMgNi_2Co_2$ + 6 % $TbCo_5$+3 % Tb_2Ni_7
6	$TbMgNiCo_3$		7.0500(1)	$Tb_{1.02}Mg_{0.98}NiCo_3$	91 % $TbMgNiCo_3$ + 2 % Tb_2Ni_7+6 % Tb_2Co_7
7	$TbMgCo_4$	8 h at 800 °C, then quenched in cold water	7.0741(1)* 7.0778(1)	$Tb_{1.07}Mg_{0.93}Co_4$	100 % $TbMgCo_4$
8	$TbMgCo_4$	12 h at 550 °C, then 1 h at 980 °C, 2 h at 1000 °C, 20 h 900 °C and 10 h at 750 °C	7.0755(2)	$Tb_{1.04}Mg_{0.96}Co_4$	~99 % $TbMgCo_4$ + 1 % Mg
9	$TbMgCo_4$	50 h at 700 °C	7.0723(2)	$Tb_{0.92}Mg_{1.08}Co_4$	82 % $TbMgCo_4$ + 17 % Tb_2Co_7 + 1 % $TbCo_5$
10	$TbMgCo_4$	18 h at 800 °C, then 48 h at 600 °C	7.0763(1)	$Tb_{0.91}Mg_{1.09}Co_4$	96 % $TbMgCo_4$ + 4 % MgO

* – data from SRXRD (Synchrotron Radiation X-Ray Diffraction).

Hydrogen absorption-desorption properties of the alloys were characterized using a Sieverts type apparatus. The samples were activated by heating up to 200 °C in dynamic vacuum, cooled to room temperature and then hydrogenated with high purity hydrogen gas (99.999%). Pressure–Composition–Temperature (*PCT*) curves were measured under H_2 pressures from 0.01 to 100 bar at temperatures between 25 and 50 °C. The hydride sample holder was put into liquid nitrogen (77 K) for 30 minutes at a final internal pressure. Then the pressure in the sample-holder was gradually reduced to 1 bar and the hydrogenated samples exposed to air, heated to room temperature and removed from the sample holder. This procedure allows to passivate the surface by a thin oxide layer and to avoid fast hydrogen desorption at ambient pressure and temperature. Then the samples were transferred into small containers and placed in liquid N_2 or fridge to keep them for further different investigations. 6 g of $TbMgCo_4$ deuteride has been prepared from sample No. 10 (Table 1) for the investigation by neutron powder diffraction (NPD).

The XRD patterns of the hydrides were repeatedly measured on air to follow the partial decomposition with time into initial compounds.

Synchrotron radiation X-ray diffraction experiments (SRXRD) have been performed at room temperature on CRISTAL beam line of synchrotron SOLEIL for selected hydrides and deuterides. The powders were placed in

glass capillaries (0.2-0.3 mm). The wavelength of the monochromatic beam, refined with a LaB_6 reference, was λ = 0.6713 Å. A Mythen multidetector has been used to obtain a good statistic on a large Q range (1-12.7 $Å^{-1}$).

In situ Synchrotron Radiation XRD study was carried out on the BM01B line at the European Synchrotron Radiation Facility (ESRF, Grenoble, France) on high-resolution diffractometer using monochromatic X-ray beam (λ = 0.5012 ± 0.0002 Å). Thin quartz capillary (diameter 0.5 mm, wall thickness 0.01 mm) was filled by the investigated alloy powder (2–5 mg, sample No.7) and placed in a special quartz cell mounted on a goniometer head and connected to the gas system through a flexible plastic tube. The heating and cooling of the sample was performed using a programmable cryofluidic system with working temperature range -196–230 °C. Initially the sample was heated in a dynamic vacuum to 150 °C and when one reaches this temperature, the hydrogen gas (99.999% purity) was introduced into a quartz cell. Under these conditions, "activation" of the alloy was done and a solid solution of hydrogen in IMC was formed. Further, the sample was slowly cooled (5 K/min) to room temperature to achieve the hydride formation.

Neutron powder diffraction (NPD) data for $TbMgCo_4D_6$ deuteride has been collected at room temperature using the high resolution 3T2 powder diffractometer at the Laboratoire Léon Brillouin (LLB, CEA, Saclay, France) with λ = 1.225 Å (angular range $4.5° \leq 2\theta \leq 121°$ and a step of 0.05°). Deuteride has been transported to the neutron reactor in a cooled reservoir and transferred into vanadium container. Rietveld refinements of the X-ray and neutron data were done with FullProf suite software[24].

DSC experiments were performed using Discovery DSC 25 of TA instrument. The heating rate was 5 or 10 K/min.

3. Results and discussion

3.1. Synthesis and crystal structure refinement of $TbMgNi_{4-x}Co_x$

$TbMgNi_{4-x}Co_x$ (x = 0–4) alloys with stoichiometric compositions 1:1:4 have been synthesized (Table 1). Such $RMgT_4$ ternary IMC crystallize in the $SnMgCu_4$ structure type, which is an ordered variant of the $AuBe_5$ type (space group $F\bar{4}3m$). They can be considered also as derivatives of the cubic $MgCu_2$ type structure (space group $Fd\bar{3}m$). Cell parameter of $TbMgNi_4$ compound synthesized in this work, 7.02047(6) Å, is in good agreement with literature data, 7.0365(4) Å[25]. The unit cell volume V of $TbMgNi_{4-x}Co_x$ IMC increases almost linearly versus Co content (Fig. 1), with a deviation for x = 3. However, the chemical composition of this IMC measured by WDS is $Tb_{0.96(1)}Mg_{1.05(2)}Ni_{1.03(3)}Co_{2.96(4)}$ in agreement with the nominal composition and cannot explain this deviation. Previous studies reported partial disordering of rare earth and magnesium atoms between 4*a* and 4*c* sites in the structures of $RMgNi_{4-x}Co_x$ compounds[19-21,25]. In this work a small deviation from the 1:1:4 stoichiometry has been observed as well. At the beginning, crystal structure refinements have been performed assuming ordered 1:1:4 composition. However, this resulted in a negative B_{iso} parameter for Mg atoms in 4*c* position for $TbMgNi_{4-x}Co_x$ (x = 2, 3 and 4). Refinements of site occupancies gave us positive value of B_{iso} and Mg concentration in the range 0.92(1)–0.98(1) Mg atoms per formula unit (at./f.u.). Apparently, it is related to the difficulty to prepare stoichiometric Mg-based alloys, as Mg can easily evaporate at synthesis conditions. According to the different

synthesis protocols, undesirable impurity phases still exist in some of the $TbMgNi_{4-x}Co_x$ alloys (TbT_5 and Tb_2T_7). Crystallographic parameters of $TbMgNi_{4-x}Co_x$ (x = 0–4) ternary compounds obtained from X-ray diffraction data are given in Tables 1 and S1 (supplementary material). SRXRD pattern of $TbMgCo_4$ is presented in Fig. S1 for comparison with XRD patterns of the selected hydrides.

The formation of ordered $RMgCo_4$ compounds was also found for R = Ce[19] and Y[20], but not for R = La[22], Pr[23], Nd[21]. It is explained by the small solubility of Mg in RCo_2 as only 6 at. % of Mg is found for R = Nd[12], while it reaches 16–20 at. %. for R = Y[26] and Tb[27]. Co-containing alloys can be synthesized by Co for Ni substitution in the $RMgNi_{4-x}Co_x$ IMC, but are limited to x = 3 Co at./f.u. for light R = La[22], Pr[23], Nd[21]. The formation of $NdMgNi_{4-x}Co_x$ compounds (x = 0–3) with cubic structure has been found, whereas $NdMgCo_4$ does not form[21].

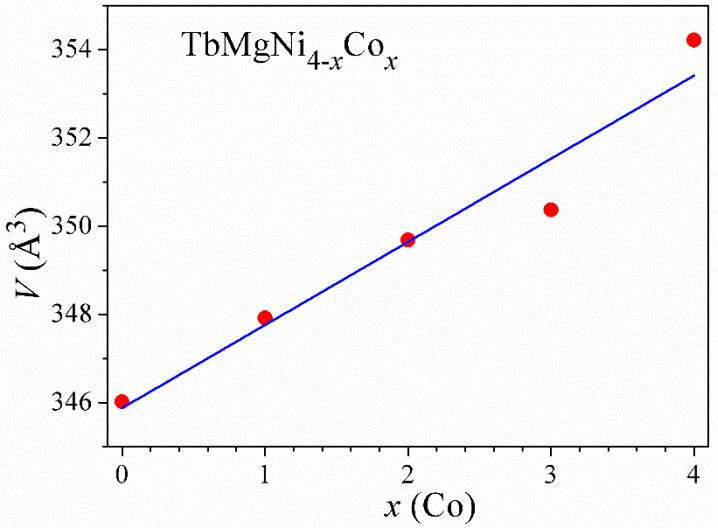

Fig. 1. Change of the unit cell volume with Co content for $TbMgNi_{4-x}Co_x$ (x = 0–4) compounds.

3.2. Hydrogen absorption properties of the $TbMgNi_{4-x}Co_x$

After an activation pretreatment at 200 °C under primary vacuum, all the pseudo-binary $TbMgNi_{4-x}Co_x$ (x = 0–4) alloys readily absorb hydrogen at room temperature. Hydrogen storage capacity reaches 3.3 to 6 H at./f.u. depending on the Co content. The absorption isotherms at 25°C are shown in Fig. 2*a*. All the compounds present a plateau corresponding to $\alpha \rightarrow \beta$ phase transformation with equilibrium pressure decreasing from 10.9 to 1 bar of H_2 for $TbMgNi_4$ to $TbMgCo_4$ compounds respectively (Fig. 2*b*). It was not possible to observe second plateaus in *PCT* curves of $TbMgNi_4$ and $TbMgNi_3Co$ because the maximum pressure of the setup was limited to 100 bar H_2 while higher plateau pressures are expected. A second plateau corresponding to $\beta \rightarrow \gamma$ phase transformation was nevertheless observed for the $TbMgNi_{4-x}Co_x$ compounds with larger Co content (x = 2, 3 and 4). It is clearly visible that with increasing Co content and therefore cell volume of the alloys, the equilibrium pressure of the first plateaus decreases as expected from the inverse relationship between equilibrium pressure and cell volume. The same trend has been observed for the second plateau. In addition, the pressure difference between first and second plateaus decreases as a function of Co content. Dependences of the equilibrium pressure versus the Co content are presented in Fig. 2*b*. The pressure of the first plateau changes sharply for x = 0 to 2 and with a smaller slope for x = 2 to 4. The equilibrium pressure of the second plateaus decreases sharply as x increases from 2 to 4.

An interesting finding has been observed for $TbMgCo_4$–H_2 system. At T = 25 °C two plateaus exist, while at T = 50 °C only one prolongated plateau has been observed (Fig. 2*c*). However a change of slope is seen in the absorption and desorption curve at 50 °C for ~3.6 H at./f.u. Its shows the sensitivity of the formation of this *β*-hydride to the temperature which critical temperature of formation should be between 25 and 50 °C.

First hydrogenation curves of selected alloys are presented in Fig. 2*d*. An improvement of the kinetics of hydrogen absorption was observed for increasing Co content. The difference in the hydrogenation curves at different Co-content primarily resulted from the difference of rate in the short initial period of reaction.

Reaction kinetic curves were analyzed with Johnson–Mehl–Avrami (JMA) equation[28]:

$$ln\big(-ln(1-\xi)\big) = \ln(k) + n \cdot ln(t) \text{ or } y = 1 - exp(-(k \cdot x)^n)$$

ξ stands for the reaction fraction after a certain period of reaction time *t*; *k* is the reaction rate constant; and *n* is the Avrami exponent, related to the system geometry.

The values of the reaction rate constant *k* and the Avrami exponent have been calculated for different compounds from JMA equation from the best fits of the kinetic data under isothermal conditions (Table 2). For all compounds, hydrogenation region at 10 bar H_2 was taken into account. It is noticeable that both *k* and *n* increase with the Co content. The obtained data shows that the hydrogenation rate increases with Co content. Similar results were obtained for Pr- and $Pr_{0.5}La_{0.5}$-containing alloys[23].

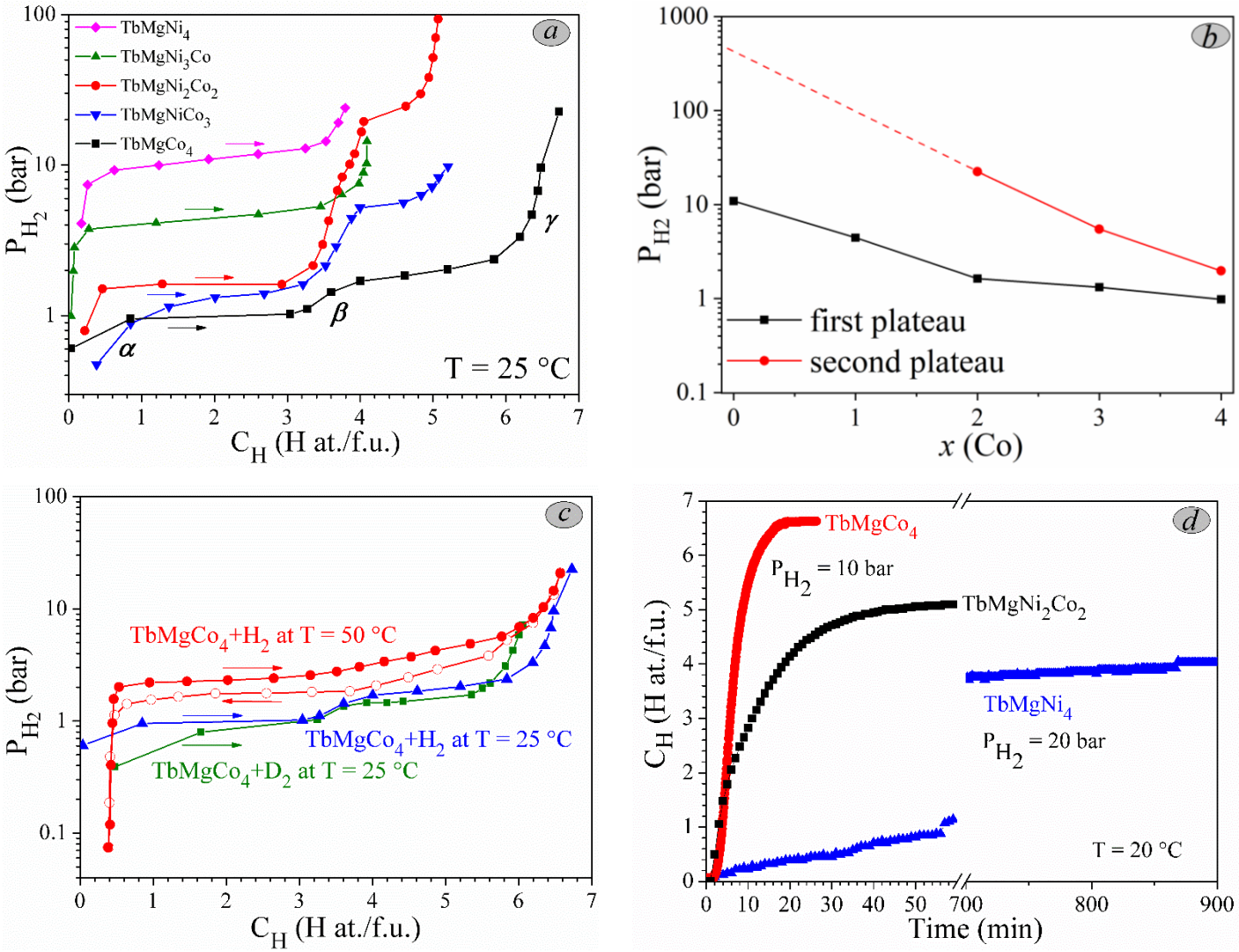

Fig. 2. Hydrogenation properties of the $TbMgNi_{4-x}Co_x$ alloys: hydrogen absorption isotherms at 25 °C (*a*); evolution of the equilibrium pressure with *x*(Co) (*b*), comparison of *PCT* curves for the $TbMgCo_4$–H_2 system at 25 and 50°C (*c*), and first hydrogenation curves for the $TbMgNi_{4-x}Co_x$ (*d*).

Table 2. JMA kinetic parameters of the formation of $TbMgNi_{4-x}Co_x$ hydrides.

Compound	ln(*k*)	*k*	*n*	R^2
$TbMgNi_4$	-9.3763	$8.47 \cdot 10^{-5}$	0.87(1)	0.9855
$TbMgNi_2Co_2$	-6.6003	$1.36\ 10^{-3}$	1.04(1)	0.9983
$TbMgCo_4$	-6.1193	$2.1\ 10^{-3}$	2.16(3)	0.9947

In all $RMgNi_{4-x}Co_x$–H_2 systems, the hydrogen capacity and kinetics of the hydride formation is improved by introduction of Co[20-23,29,30]. *PCT* curves with two plateaus for the $TbMgNi_{4-x}Co_x$ compounds ($x \geq 2$) resemble those obtained for isostructural $LaMgNi_4$[31] and $CeMgCo_4$[19] compounds, where formation of the *α*-, *β*-, *γ*-hydrides have been also observed. For $RMgNi_{4-x}Co_x$ compounds[19-23,29,30] only one plateau has been observed. Moreover, for the $(Nd,Pr)_{1-y}La_yMgNi_{4-x}Co_x$ alloys, La and Co substitution initiates an easiest way to observe the $\beta \rightarrow \gamma$ transformation at 10 bar H_2[22,23]. For $YMgCo_4$ compound, an extended plateau was observed in the temperature range 20–60 °C[20] like at 50 °C for $TbMgCo_4$ in this work.

According to the variation of the equilibrium pressures (Fig. 2*b*), the second plateau pressures of $TbMgNi_{4-x}Co_x$ could be near 400 and 110 bar for $x = 0$ and 1 respectively. To confirm this assumption experiment at higher hydrogen pressure should be done and results of first principles calculations are presented in section 3.5. Interesting, that theoretical calculations suggested that $RMgNi_4H_4$ can transform into $RMgNi_4H_6$ at 2.64 and 85 kbar H_2 for R = Sm and Gd respectively[32]. On the other hand, $CeMgCo_4$ displays a second plateau below 100 bar H_2[19], whereas hydrogenation of the $CeMgNi_4$ alloy leads to an alloy decomposition[33].

3.3. Crystal structures of the $TbMgNi_{4-x}Co_x$-based hydrides

Hydrides of the $TbMgNi_{4-x}Co_x$ compounds with $x = 0$, 1, 2, 3 and 4 were exposed to air to passivate the surface and characterized by XRD and SRXRD. Rietveld refinements of the different XRD patterns of selected $TbMgNi_{4-x}Co_x$ hydrides and deuterides are shown in Figures S1 and S2. The structures of different β- and γ-hydrides are presented in Table 3. First, it was found that the hydrogenation of $TbMgNi_{4-x}Co_x$ with $x = 0$, 1, 2 and 3 leads to an orthorhombic deformation (space group $Pmn2_1$) of the original cubic structure (space group $F\bar{4}3m$) with a cell volume expansion of 12.6–14.7 % (Table 3 and Fig. 3*a*). However, it was observed that $TbMgCo_4H_{3.3}$ crystallizes in a monoclinic structure (space group Pm, a = 5.4091(8) Å, b = 5.0035(6) Å, c = 7.3606(9) Å, β = 96.18(1)°) (Figure S1). This monoclinic structure corresponds to a distortion of the orthorhombic cell and can be obtained by a lowering of the crystal symmetry from $Pmn2_1$ (No. 31) to Pm (No. 6). Full resolution of this new structure with D-atom location, will be done later by NPD measurement. The variation of β-hydride cell parameters versus Co content is presented in Fig. 3*b*. a and b cell parameters decrease monotonously, while c sharply increases up to $x = 2$ and saturates at 3 Co at/f.u. Further hydrogenation of the $TbMgNi_{4-x}Co_x$ alloys yields cubic γ-hydrides for x = 2, 3 and 4. These hydrides retain initial cubic symmetry of the parent compound with isotropic expansion of the unit cell of 17.9–22.3 % (Table 3). Synthesis of γ-hydrides with cubic structure for the $TbMgNi_{4-x}Co_x$ compounds with $x = 0$ and 1 would require higher hydrogen pressure as previously discussed.

Subsequently, isotope influence on phase structure and stability has been observed in the $TbMgNiCo_3$–$(H,D)_2$ system. $TbMgNiCo_3H_{5.2}$ hydride is unstable versus time and decomposes very fast into orthorhombic phase with y = 3.7 H/f.u. On the other hand, $TbMgNiCo_3D_{5.4}$ deuteride remains stable and keep a cubic structure. XRD patterns for hydrides and deuterides are compared in Fig. 3*c*. $TbMgCo_4$ absorbs 6.6 H at./f.u. at 9.5 bar H_2, but desorb hydrogen down to 5.2 H at./f.u. at 1 bar H_2. Cell parameter for the cubic hydride $TbMgCo_4H_{5.2}$ has been determined by SRXRD (a = 7.5035(2) Å^3) and it is in agreement with our previous result for $TbMgCo_4H_{5.3}$[27] from XRD (a = 7.5212(9) Å^3). $TbMgCo_4D_6$ deuteride (a = 7.5663(2) Å) is also more stable than its corresponding hydride. The cubic structure of $TbMgNi_2Co_2H_{\sim 5}$ hydride was observed after very fast scan.

Cell volume (V) variations versus Co content are presented in Fig. 3*d*. The cell volume of $TbMgNi_{4-x}Co_x$ β-hydrides increases from $x = 0$ to 2, decreases abruptly for $x = 3$ and increases again for monoclinic hydride with $x = 4$. This discontinuous cell volume variation is mainly related to the variation of the c parameter with x(Co). This anomalous variation for $x = 3$ can be related to the small deviation from linearity of the initial compound cell volume (Fig. 1). The γ-deuteride (hydride) cell volume V increases continuously (volume of the $TbMgNi_2Co_2H_{\sim 5}$ hydride has been used instead of deuteride).

Table 3. Crystal structure data for the $TbMgNi_{4-x}Co_xH_y$ hydrides/deuterides (synthesized at room temperature) from Rietveld refinements of X-ray diffraction data.

Hydride	P_{final} H_2, bar	Space Group	Unit cell parameters (Å)			V(Å^3)	$\Delta V/V$, %	$\Delta V/n_H$, Å^3/at.H
			a	*b*	*c*			
β-$TbMgNi_4H_{3.8}$	24.0	$Pmn2_1$	5.0182(6)	5.4178(6)	7.2834(8)	198.02(4)	14.7	3.2
β-$TbMgNi_3CoH_{4.1}$	10.3	$Pmn2_1$	5.0074(2)	5.4060(3)	7.3225(3)	198.22(2)	14.3	3.0
β-$TbMgNi_2Co_2H_{3.7}$	6.8	$Pmn2_1$	4.9957(5)	5.4084(6)	7.3588(7)	198.83(3)	13.7	3.0
γ-$TbMgNi_2Co_2H_{\sim5}$	52.0	$F\bar{4}3m$	7.4419(7)			412.15(7)	17.9	3.1
β-$TbMgNiCo_3H_{3.7}$	2.4	$Pmn2_1$	4.981(1)	5.390(2)	7.350(2)	197.3(1)	12.6	3.0
γ-$TbMgNiCo_3H_{5.2}$	9.8	***fast decomposition into β-$TbMgNiCo_3H_{3.7}$***						
γ-$TbMgNiCo_3D_{5.4}$	7.3	$F\bar{4}3m$	7.4785(3)			418.26(3)	19.4	3.1
β-$TbMgCo_4H_{3.3}$	1.5	Pm	5.4091(8)	5.0035(6) β=96.18(1)°	7.3606(9)	198.05(5)	11.8	3.2
γ-$TbMgCo_4H_{5.2}$	2.3	$F\bar{4}3m$	7.5035(2)			422.47(2)	19.3	3.3
γ-$TbMgCo_4D_6$	7.1	$F\bar{4}3m$	7.5663(2)			433.15(2)	22.2	3.3

Statistical mixture of Mg/Tb were taken as it was calculated for IMC and fixed for hydrides.

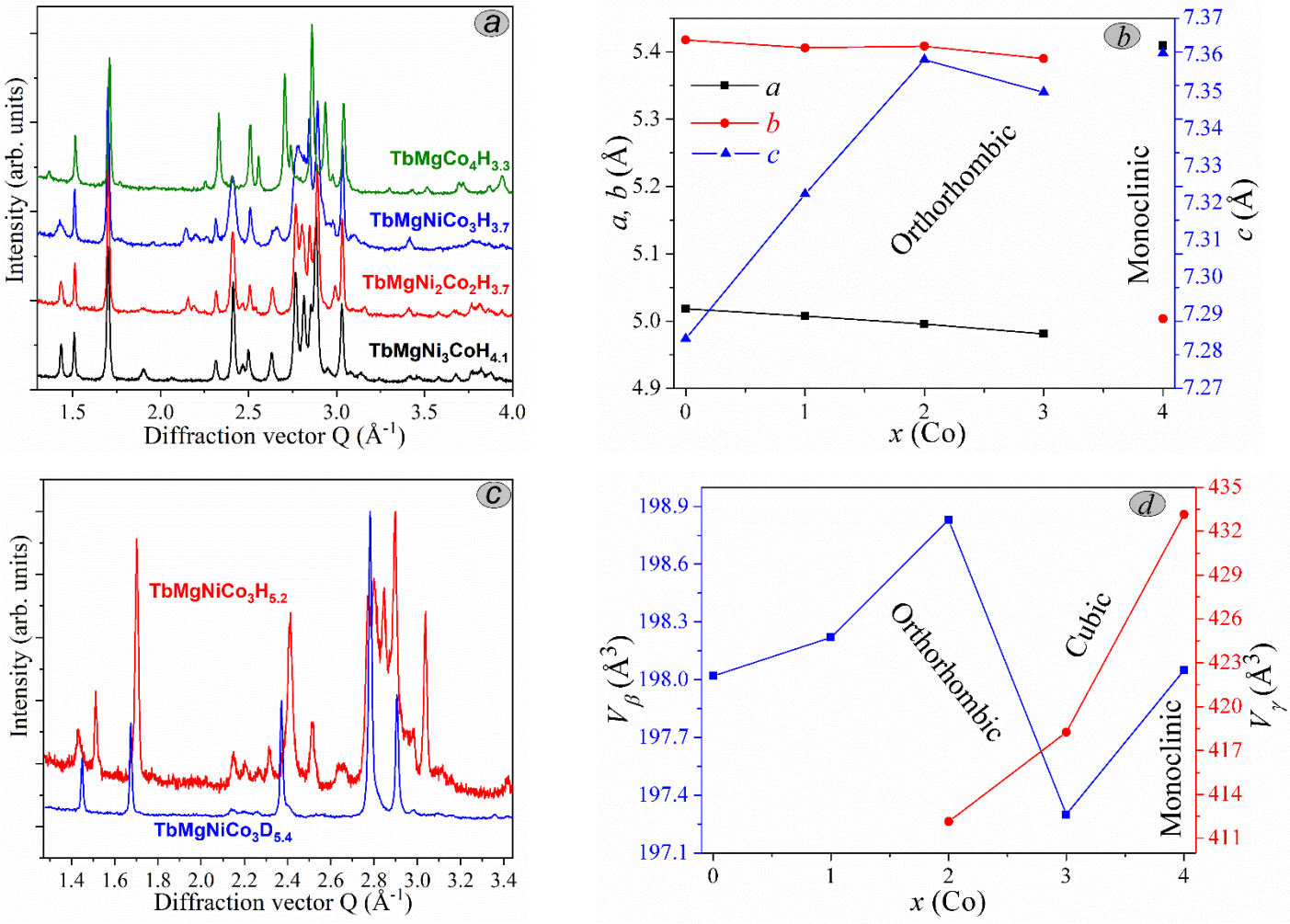

Fig. 3. XRD patterns of the selected $TbMgNi_{4-x}Co_x$ hydrides (*a*,*b*) and evolution of the cell parameters versus Co content (*c*,*d*).

Crystal structure of $TbMgCo_4D_6$ deuteride has been studied in more detail by neutron powder diffraction. Saturated $TbMgCo_4D_{6.1}$ deuteride has been obtained at room temperature and 7.1 bar D_2. According to volumetric measurement, the final concentration of the deuterium in the IMC at 1 bar D_2 was 6 D at./f.u. This deuteride keeps the cubic structure of the parent compound with a large cell volume expansion ($\Delta V/V$ = 22.3 %). Several XRD and SRXRD measurements have showed that $TbMgCo_4D_6$ remains stable over several months contrary to hydrides of Ni reach compounds which decompose during storage.

The structural parameters determined from XRD and NPD datasets are reported in Table 4. Fig. 4 shows the refined neutron diffraction pattern at room temperature and unit cell projection of this deuteride. As starting structural model in Rietveld refinements of the deuteride NPD pattern, we used structural parameters of $TbMgCo_4D_6$ obtained from XRD data. The lattice parameters determined of $TbMgCo_4D_6$ determined from NPD are close to those determined by XRD. The positions of the deuterium atoms have been found using differential Fourier method. The deuterium atoms partially occupy two types of interstitial sites: 87 % D atoms are located in D1 which form a Tb_2MgCo_2 octahedra and 13 % (D2) are located in Co_4 tetrahedra. Total deuterium content obtained from Rietveld refinements is 5.9(2) D at./f.u. in good agreement with the value of 6.0 D at./f.u. measured from pressure variation. Similar type of R_2MgT_2 and T_4 coordination of D atoms was observed in $CeMgCo_4D_{4.21}$[19] and $LaMgNi_4D_{4.85}$[29] deuterides.

Mg–D and Co–D distances are 1.819(1) Å and 1.614(1)–1.684(2) Å respectively. These value are comparable to those obtained for $CeMgCo_4D_{4.21}$[19] ($d_{Mg\text{-}D}$ = 1.835 Å and $d_{Co\text{-}D}$ = 1.646 Å) where one 24*g* position is filled. Mg–D distances in $LaMgNi_4D_{4.85}$[31] and $NdMgNi_4D_{3.6}$[34], $PrMgNi_4D_4$ and $Pr_{0.6}Mg_{1.4}Ni_4D_{3.6}$[35] are in the range 1.856–2.221 Å.

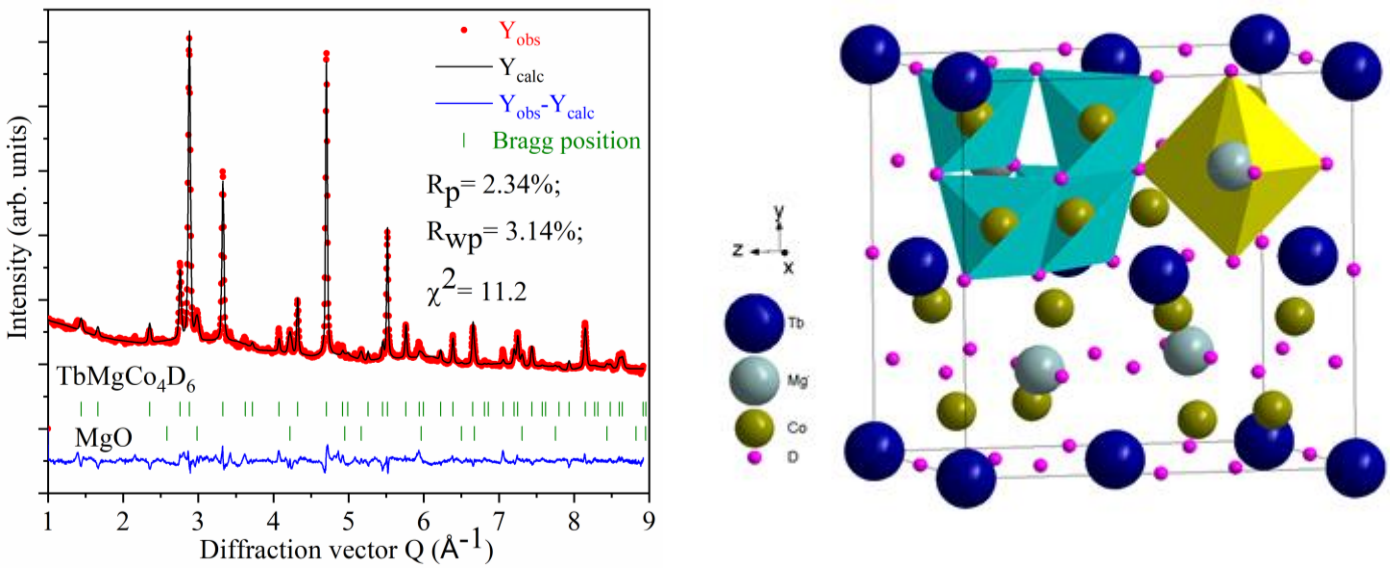

Fig. 4. Refined NPD pattern (1 – 97 wt.% $TbMgCo_4D_6$, 2 – 3 wt.% MgO) and unit cell projection of the $TbMgCo_4D_6$ deuteride with an environment of D atoms around Co and Mg.

Table 4. Crystallographical parameters of the $TbMgCo_4D_6$ deuteride from Rietveld refinements of XRD and NPD data.

Deuteride	$TbMgCo_4D_6$	
Refinement	XRD	NPD
Space group	$F\bar{4}3m$ (No. = 216)	
Unit cell parameters: a, Å V, Å^3	 7.5663(2) 433.15(2)	 7.5553(2) 431.28(2)
$\Delta V/V$, %	~22.0	
Atomic positions:		
Tb in 4*a* (0, 0, 0)		
*n_{Tb}/n_{Mg}	0.84(-)Tb/0.16(-)Mg	
B_{iso}, Å^2	1.58(7)	2.23(11)
Mg in 4*c* (1/4, 1/4, 1/4)		
*n_{Mg}/n_{Tb}	0.93(-)Mg/0.07(-)Tb	
B_{iso}, Å^2	3.4(3)	2.16(9)
Co in 16*e* (*x*, *x*, *x*)		
x	0.6236(2)	0.6233(3)
B_{iso}, Å^2	1.19(6)	1.91(7)
D1 in 24*g* (*x*, 1/4, 1/4)		
x		0.4904(4)
n		0.86(1)
D2 in 4*b* (1/2, 1/2, 1/2)		
n		0.76(1)
B_{iso}, Å^2 for all D		3.56(4)
Calculated D content		5.9(2)
Volumetric capacity, D at./f.u.	6.0	
R-factors		
R_p, %	1.21	2.34
R_{wp}, %	1.59	3.14
χ^2	1.72	11.2
Shortest Me–D distances, Å		
Mg–D1 Co–D2 Co–D1		1.819(1) 1.614(1) 1.684(2)

*Statistical mixtures of Mg/Tb were taken as it was calculated for IMC and fixed for deuteride.

3.4. DSC studies of the $TbMgNi_{4-x}Co_xH_y$ hydrides

DSC studies have been performed to determine the enthalpy and temperature of desorption (ΔH_{des}, T_{des}) which are related to the hydride stability. Measured weight capacity, ΔH_{des} and T_{des} obtained from DSC experiments are summarized in Table 5.

It was found that T_{des} and ΔH_{des} for the orthorhombic β-$TbMgNi_{4-x}Co_xH_y$ hydrides (x = 0–3 and y = 3.7–4.1) varies in a narrow T and ΔH_{des} range: 69.5–84.4 °C and 18.3–31.6 kJ/mol H_2, respectively. The hydride of $TbMgNi_4$ has the lowest stability among studied hydrides. The β-$TbMgCo_4H_{3.3}$ has the highest values of T_{des} (117.1 °C) while the highest ΔH_{des} was found for the β-$TbMgNiCo_3H_{3.7}$ hydride (31.6 kJ/mol H_2). The results of DSC experiments (Table 5) show that β-hydrides more stable than γ-hydrides. These observations agree with the

results of the *PCT* measurements, demonstrating that increasing Co content leads to a significant decrease in the equilibrium plateau pressure and increasing stability of the hydrides (Fig. 2*a*).

The values of ΔH_{des} are close to that for $LaNi_5$ hydride, which enthalpy of formation is ranging from about 29 to 32 kJ/mol H_2[36]. The values of the hydrogen absorption enthalpy determined from the slope of van't Hoff plot for $YMgNi_{4-x}Co_x$–H_2 systems varies from 27.9 to 33.1 $kJmol^{-1}$ H_2[20].

Table 5. Comparison of desorption temperature and enthalpy of the $TbMgNi_{4-x}Co_xH_y$ hydrides.

Hydride	C_H, wt. %	T_{onset}, °C	Enthalpy, J/g	Enthalpy, kJ/mol $H(D)_2$
β-$TbMgNi_4H_{3.8}$	0.91	69.5	82.8	18.3
β-$TbMgNi_3CoH_{4.1}$	0.98	84.4	138.5	28.5
β-$TbMgNi_2Co_2H_{3.7}$	0.88	70.7	129.5	29.7
β-$TbMgNiCo_3H_{3.7}$	0.88	76.2	138.1	31.6
γ-$TbMgNiCo_3D_{5.4}$	1.28	93.4	166.0	26.1
β-$TbMgCo_4H_{3.3}$	0.79	117.1	113.5	29.0
γ-$TbMgCo_4H_{5.3}$	1.27	99.6	181.7	28.8

3.5. DFT Calculations of $TbMgNi_{4-x}Co_x$ compounds and $TbMgNi_{4-x}Co_xH_6$ hydrides

First principles calculations were performed on $TbMgNi_{4-x}Co_x$ compounds and cubic $TbMgNi_{4-x}Co_xH_6$ hydrides, with a given model for x = 0, 2 and 4. The partial substitution cells (x = 2) were obtained by choosing the most randomized distribution of the 16 atoms (8 Co + 8 Ni) in 16*e* site of $F\bar{4}3m$ space group. Similar to the Special quasirandom structure (SQS) approach[37], the cell was chosen by comparison of the correlation functions of a set of clusters (5 nearest pairs, 6 nearest triplets and 2 tetrahedra) of all possible atom configurations with the perfect randomized cell. To get a general picture of a relative and simple comparison, the hydride form was considered only in an ideal cubic model (γ-form) with a partial occupancy of H in 24*g* and 4*b* sites, representative of the experimental results of $TbMgCo_4D_6$, *i.e.* 21/24 and 3/4 atoms respectively in the conventional cell (48 atoms in total). The distribution of H was considered with relative positions far of each other with the highest symmetry possible case. As an example, the structural model of $TbMgNi_2Co_2H_6$ is given in supporting information (Table S2 and Fig S3, with additional VESTA file).

The spin polarized band structure calculations were carried out by using the DFT scheme implemented in the projector-augmented wave (PAW) method, performed with the VASP package[38,39], using the Generalized Gradient Approximation (GGA) for the exchange and correlation energy of Perdew-Burke-Ernzerhof (PBE) functional[40]. Terbium was considered with "ghost-state" approach using a special pseudopotential in which the *f* electrons are kept frozen in the core (only 9 valence electrons). A plane wave basis set with a cutoff energy of 600 eV was used in all calculations converging within 0.1 meV in the total energy.

From the energies difference related to pure elements in their reference state, the heats of formation of intermetallics and hydrides are given in Table 6. In agreement with the conventional Miedema rules for hydride, the less stable compound (richer in Co) forms the most stable hydride. The opposite applies to the Ni-based

compound to be very stable (about -40 kJ/mol) whereas the $TbMgNi_4H_6$ hydride is not stable in ambient conditions (P_{eq} > 400 bar).

Table 6. Heat of formation of $TbMgNi_{4-x}Co_x$ compounds and $TbMgNi_{4-x}Co_xH_6$ hydrides calculated by DFT.

x	Compound	Enthalpy, kJ/mol	Hydride	Enthalpy, kJ/mol H_2
0	$TbMgNi_4$	-38.8	$TbMgNi_4H_6$	-10.9
2	$TbMgNi_2Co_2$	-24.4	$TbMgNi_2Co_2H_6$	-18.4
4	$TbMgCo_4$	-13.1	$TbMgCo_4H_6$	-18.8

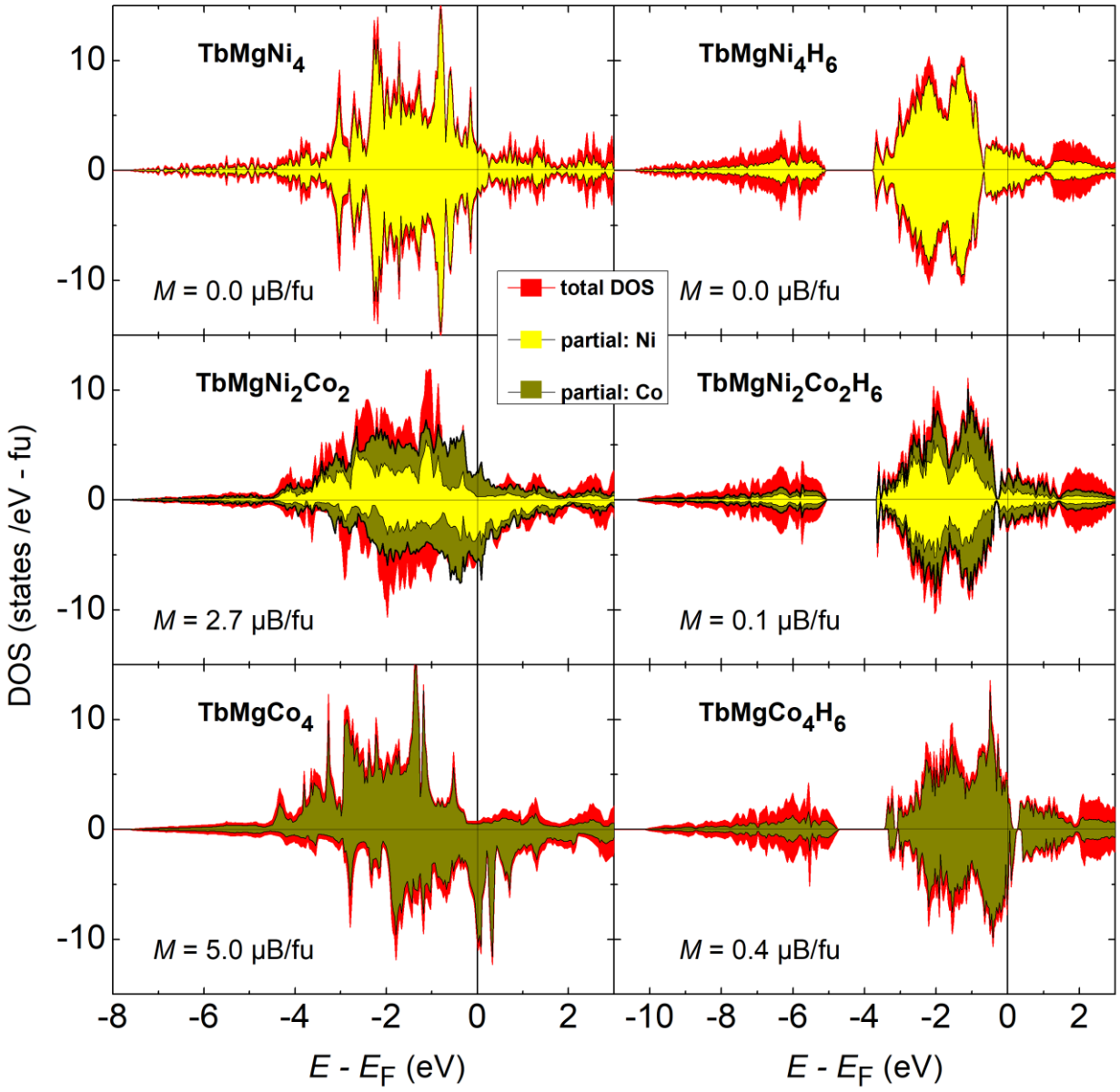

Fig. 5. Density of states of $TbMgNi_{4-x}Co_x$ compounds and $TbMgNi_{4-x}Co_xH_6$ hydrides for *x* = 0, 2, 4. Red area corresponds to the total contribution whereas yellow and green areas correspond to the Ni and Co parts respectively. The Fermi level has been chosen as the origin of energy.

The electronic structure could be analyzed from the density of states (DOS) representation given in Fig. 5. About the intermetallics, an electron depopulation of the main band is observed with the increase of *x* (increase

of Co-rate), naturally explained by the number of electrons of Ni and Co. The DOS of hydrides is typical of this kind of phase, characterized by a new broad electronic structure at low energy (around -10 to -5 eV below the Fermi level, E_F). It corresponds mostly to the 6 bands associated with metal-hydrogen bonding dominating by H–(Co,Ni) interactions. Due to the lattice expansion of the hydride (about +18 %), the Tb+Mg and transition metal interaction is weakened, the bands of the main structure are narrower and the valley separating the bonding and anti-bonding states is smeared out. Thanks to the additional electrons from H atoms, the Fermi level is shifted at higher energy for the hydrides and leads to the almost filling of the main structure in $x = 4$ whereas E_F falls in anti-bonding states for $x = 0$.

Whatever the x value, the Bader charge analysis indicated a charge transfer from Mg and Tb to H with a total charge of about 0.45 e^- for each H atom, as shown in high density region around H of the electron localization function (ELF) plotted in Fig S4 of Supporting Information. The transition metal charges are most unchanged from their elemental state.

A substantial increase of the calculated enthalpies of formation has been also observed when Ni is replaced by Co in $YMgT_4$ IMC (T = Ni, Co)[41] and Y by Nd in RMgNi$_4$ IMC (R = Y, Nd)[42]. Previously we assumed that the enthalpy of formation of $NdMgCo_4$ is possibly positive and that $NdMgCo_4$ compound and others with R = La, Pr, Nd are thermodynamically unstable. Moreover, latest publication[43] revealed good structural stability with the order: $NdMgCo_4$ > $NdMgNi_4$ > $NdMgCu_4$. Calculated cell parameter for $NdMgCo_4$ compound was 7.1078 Å. Besides, it was experimentally found that cell parameters of $NdMgNi_{4-x}Co_x$ compounds increase linearly from 7.0947(5) Å for $x = 0$ to 7.1286(6) Å for $x = 3$. By extrapolation, the cell parameter of $NdMgCo_4$ compound should be 7.1404 Å, but this compound can not be obtained. Meanwhile, calculated enthalpies of formation for $NdMgCo_4$ is -0.08 eV/atom which is close to a positive value and explaining that it is thermodynamically unstable. Finally, formation of the RMgCo$_4$ compounds depends on the nature of rare earth and Mg solubility in the binary RCo$_2$ compounds.

4. Conclusions

$TbMgNi_{4-x}Co_x$ (x = 0–4) intermetallics with $SnMgCu_4$ type cubic structure have been synthesized. Their hydrogenation properties have been studied in detail. The structural study of the alloys and their hydrides or deuterides has been performed.

$TbMgNi_{4-x}Co_x$ (x = 0–4) compounds reversibly absorb hydrogen. *PCT* curves of $TbMgNi_{4-x}Co_x$ display only one plateau (x = 0–1) whereas *PCT* curves of $TbMgNi_{4-x}Co_x$ (x = 2–4) compounds are characterized by two absorption/desorption plateaus. Thermodynamic properties of the $TbMgNi_{4-x}Co_xH_y$ (x = 0–4) hydrides were studied by *PCT* and DSC measurements. The experimental enthalpies of formation are in good agreement with the DFT calculated ones. It shows a decreasing stability of the alloys upon Co for Ni substitution and the reverse effect on the hydride as expected from the reverse stability rule. Increasing Co content in the $TbMgNi_{4-x}Co_x$ alloys leads to the lowering of desorption plateau pressure and improvement of the kinetics of hydrogen absorption.

The existence of α-, β-, γ-hydrides has been observed in the *PCT* curves. Formation of the β-hydrides is going through the orthorhombic distortion of the cubic $TbMgNi_{4-x}Co_x$ (x = 0–3) intermetallics. Moreover, β-$TbMgCo_4H_{3.3}$ has a monoclinic structure observed for the first time among $RMgNi_{4-x}Co_xH_y$ hydrides. This monoclinic structure corresponds to a distortion of the orthorhombic structure and can be obtained by a lowering of the crystal symmetry. Deuterium has been found to prevent from fast desorption compared to hydrogen. The neutron diffraction study of the $TbMgCo_4D_6$ deuteride has revealed significant structural similarity with $LaMgNi_4D_{4.85}$[31] with deuterium atoms located inside Tb_2MgCo_2 octahedra and Co_4 tetrahedra.

Acknowledgments

The author thanks to Dr. E. Leroy for his assistance with EPMA analysis. They are also thankful to E. Elkaim, K. Provost and F. Couturas for their help for the synchrotron radiation measurements on CRISTAL at SOLEIL. We are grateful to Florence Porcher for the NPD measurements performed by at the LLB. DFT calculations were performed using HPC resources from GENCI-CINES (Grant 2018-96175).

References

1. Zhang, H.; Zheng, X.; Tian, X.; Liu, Y.; Li, X. New approaches for rare earth-magnesium based hydrogen storage alloys. *Progress in Natural Science: Materials International* **2017,** *27,* 50–57.
2. Crivello, J.-C.; Denys, R. V.; Dornheim, M.; Felderhoff, M.; Grant, D. M.; Huot, J.; Jensen, T. R.; Jong, P.; Latroche, M.; Walker, G. S.; et al. Mg-based compounds for hydrogen and energy storage. *Appl. Phys. A* **2016,** *122,* 85–102.
3. Jain, I. P.; Lal, C.; Jain, A. Hydrogen storage in Mg: A most promising material. *Int. J. Hydrogen Energy* **2010,** *35,* 5133–5144.
4. Bobet, J.-L.; Gaudin, E.; Couillaud, S. *New ternary intermetallics based on magnesium for hydrogen storage: The fishing approach;* Souza, F.; Leite, E., Eds.; Nanoenergy. Springer, Cham, 2018; pp. 301–328.
5. Zhu, M.; Wang, H.; Ouyang, L. Z.; Zeng, M. Q. Composite structure and hydrogen storage properties in Mg-based alloys. *Int. J. Hydrogen Energy* **2006,** *31,* 251–257.
6. Sakintuna, B.; Lamari-Darkrim, F.; Hirscher, M. Metal hydride materials for solid hydrogen storage: A review. *Int. J. Hydrogen Energy* **2007,** *32,* 1121–1140.
7. Jain, I. P.; Jain, P.; Jain, A. Novel hydrogen storage materials: A review of lightweight complex hydrides. *J. Alloys Comp.* **2010,** *503,* 303–339.
8. Huot, J.; Ravnsbæk, D. B.; Zhang, J.; Cuevas, F.; Latroche, M.; Jensen, T. R. Mechanochemical synthesis of hydrogen storage materials. *Progress in Materials Science* **2013,** *58,* 30–75.
9. Alasmar, E.; Aubert, I.; Durand, A.; Nakhl, M.; Zakhour, M.; Gaudin, E.; Bobet, J.-L. Hydrogen generation from Mg–$NdNiMg_{15}$ composites by hydrolysis reaction. *Int. J. Hydrogen Energy* **2019,** *44,* 523–530.
10. Shtender, V. V.; Paul-Boncour, V.; Riabov, A. B.; Denys, R. V.; Zavaliy, I. Yu. Hydrogenation behavior of the R_4MgCo (R = Y, La, Nd, Tb) compounds. *J. Solid State Chem.* **2015,** *229,* 135–140.
11. Shtender, V.; Paul-Boncour, V.; Denys, R.; Zavaliy, I. Synthesis and hydriding of $R_4Mg_3Co_2$ (R = Nd and Tb) alloys. *Visnyk Lviv Univ. Ser. Khim.* **2015,** *56,* 138–144 (in Ukranian).
12. Shtender, V. V.; Zelinska, O. Ya.; Pavlyuk, V. V.; Denys, R. V.; Paul-Boncour, V.; Zavaliy, I. Yu.; Marciniak, B.; Różycka-Sokołowska, E. Phase equilibria in the Nd–Mg–Co system at 300 and 500 °C, crystal structure and hydrogenation behavior of selected compounds. *Intermetallics* **2017,** *87,* 61–69.
13. Mašková, S.; Chotard, J.-N.; Denys, R. V.; Miliyanchuk, K.; Yartys, V.; Giovannini, M.; Akselrud, L.; Halevy, I.; Prokleška, J.; Havela, L. $Nd_2Ni_2MgH_8$ hydride: Synthesis, structure and magnetic properties. *Intermetallics* **2017,** *87,* 13–20.
14. Denys, R. V.; Riabov, A. B.; Yartys, V. A.; Sato, M.; Delaplane, R. G. Mg substitution effect on the hydrogenation behaviour, thermodynamic and structural properties of the La_2Ni_7–$H(D)_2$ system. *J. Solid State Chem.* **2018,** *181,* 812–821

15. Iwase, K.; Terashita, N.; Mori, K.; Tashiro, S.; Yokota, H.; Suzuki, T. Effects of Mg substitution on crystal structure and hydrogenation properties of $Pr_{1-x}Mg_xNi_3$. *Int. J. Hydrogen Energy* **2014,** *392,* 12773–12777.
16. Shtender, V. V.; Denys, R. V.; Paul-Boncour, V.; Zavaliy, I. Yu.; Verbovytskyy, Yu. V.; Taylor, D. D. Crystal structure, hydrogen absorption-desorption behaviour and magnetic properties of the $Nd_{3-x}Mg_xCo_9$ alloys. *J. Alloys Comp.* **2017,** *695,* 1426–1435.
17. Oesterreicher, H.; Bittner, H. Hydride formation in the $La_{1-x}Mg_xNi_2$. *J. Less-Common Met.* **1980,** *73,* 339–344.
18. Verbovytskyy, Yu. V.; Zavaliy, I. Yu. New metal-hydride materials based on $R_{2-x}Mg_xNi_4$ alloys for chemical current sources. *Mater. Sci.* **2017,** *52,* 747–759.
19. Denys, R. V.; Riabov, A. B.; Cerny, R.; Koval'chuk, I. V.; Zavaliy, I. Yu. New $CeMgCo_4$ and Ce_2MgCo_9 compounds: Hydrogenation properties and crystal structure of hydrides. *J. Solid State Chem.* **2012,** *187,* 1–6.
20. Shtender, V. V.; Denys, R. V.; Paul-Boncour, V.; Riabov, A. B.; Zavaliy, I. Yu. Hydrogenation properties and crystal structure of $YMgT_4$ (*T* = Co, Ni, Cu) compounds. *J. Alloys Comp.* **2014,** *603,* 7–13.
21. Shtender, V. V.; Denys, R. V.; Paul-Boncour, V.; Verbovytskyy, Yu. V.; Zavaliy, I. Yu. Effect of Co substitution on hydrogenation and magnetic properties of $NdMgNi_4$ alloy. *J. Alloys Comp.* **2015,** *639,* 526–532.
22. Verbovytskyy, Yu. V.; Shtender, V. V.; Hackemer, A.; Drulis, H.; Zavaliy, I. Yu.; Lyutyy, P. Ya. Solid-gas and electrochemical hydrogenation properties of the $La_{1-x}Nd_xMgNi_{4-y}Co_y$ alloys. *J. Alloys Comp.* **2018,** *741,* 307–314.
23. Oprysk, V. O.; Verbovytskyy, Yu. V.; Shtender, V. V.; Lyutyy, P. Ya.; Zavaliy, I. Yu. The $Pr_{1-x}La_xMgNi_{4-y}Co_y$ alloys: Synthesis, structure and hydrogenation properties. *Solid State Sciences* **2018,** *84,* 112–119.
24. Rodriguez-Carvajal, J. Recent developments of the program FULLPROF, in: Commission on Powder Diffraction (IUCr), *Newsletter* **2001,** *26,* 12–19.
25. Linsinger, S.; Eul, M.; Schwickert, C.; Decourt, R.; Chevalier, B.; Rodewald, U. Ch.; Bobet, J.-L.; Pöttgen, R. Structure, homogeneity ranges, magnetic and electrical properties of the ordered Laves phases $RENi_4Mg$ with $MgCu_4Sn$ type structure. *Intermetallics* **2011,** *19,* 1579–1585.
26. Shtender, V. V.; Pavlyuk, V. V.; Zelinska, O. Ya.; Nitek, W.; Paul-Boncour, V.; Dmytriv, G. S.; Łasocha, W.; Zavaliy, I. Yu. The Y–Mg–Co ternary system: Alloys synthesis, phase diagram at 500 °C and crystal structure of the new compounds. *J. Alloys Comp.* **2020,** *812,* 152072.
27. Shtender, V. V.; Denys, R. V.; Zavaliy, I. Yu.; Zelinska, O. Ya.; Paul-Boncour, V.; Pavlyuk, V. V. Phase equilibria in the Tb–Mg–Co system at 500 °C, crystal structure and hydrogenation properties of selected compounds. *J. Solid State Chem.* **2015,** *232,* 228–235.
28. Avrami, M. Kinetics of phase change. I General theory. *J. Chem. Phys.* **1939,** *7,* 1103–1112.
29. Sakaki, K.; Terashita, N.; Tsunokake, S.; Nakamura, Y.; Akiba, E. InSitu X-ray diffraction study of phase transformation of $Mg_{2-x}Pr_xNi_4$ during hydrogenation and dehydrogenation (x = 0.6 and 1.0). *J. Phys. Chem. C* **2012,** *116,* 1401–1407.
30. Czub, J.; Shtender, V. V.; Przewoźnik, J.; Zarzecka, A.; Hoser, A.; Gondek, Ł. On the properties of the novel $CeMgNi_2T_2$ (*T* = Co, Cu) alloys and their hydrides. *J. Alloys Comp.* **2020,** *814,* 152244.
31. Chotard, J.-N.; Sheptyakov, D.; Yvon, K. Hydrogen induced site depopulation in the $LaMgNi_4$-hydrogen system. *Z. Kristallogr.* **2008,** *223,* 690–696.
32. Sakaki, K.; Terashita, N.; Tsunokake, S.; Nakamura, Y.; Akiba, E. Effect of rare earth elements and alloy composition on hydrogenation properties and crystal structures of hydrides in $Mg_{2-x}RE_xNi_4$. *J. Phys. Chem. C* **2012,** *116,* 19156–19163.
33. Roquefere, J.-G.; Matar, S. F.; Huot, J.; Bobet, J.-L. X-ray/neutron diffraction studies and ab initio electronic structure of $CeMgNi_4$ and its hydride. *Solid State Sciences* **2009,** *11,* 1971–1978.
34. Guénée, L.; Favre-Nicolin, V.; Yvon, K. Synthesis, crystal structure and hydrogenation properties of the ternary compounds $LaNi_4Mg$ and $NdNi_4Mg$. *J. Alloys Comp.* **2003,** *348,* 129–137.
35. Sakaki, K.; Terashita, N.; Kim, H.; Proffen, T.; Majzoub, E.H.; Tsunokake, S.; Nakamura, Y.; Akiba, E. Crystal structure and local structure of $Mg_{2-x}Pr_xNi_4$ (x = 0.6 and 1.0) deuteride using in situ neutron total scattering. *Inorg. Chem.* **2013,** *52,* 7010–7019.
36. Schlapbach, L.; Züttel, A. Hydrogen-storage materials for mobile applications. *Nature* **2001,** *414,* 353–358.
37. Zunger, A.; Wei, S. H.; Ferreira, L. G.; Bernard, J. E. Special quasirandom structures. *Phys. Rev. Lett.* **1990,** *65,* 353–356.
38. Kresse, G.; Furthmüller, J. Efficient iterative schemes for ab initio total-energy calculations using a plane-wave basis set. *Phys. Rev. B* **1996,** *54,* 11169–11186.

39. Kresse, G.; Joubert, D. From ultrasoft pseudopotentials to the projector augmented-wave method. *Phys. Rev. B* **1999,** *59*, 1758–1775.
40. Perdew, J. P.; Burke, K.; Ernzerhof, M. Erratum: Generalized gradient approximation made simple phys. *Rev. Lett. American Phys. Society* **1997,** *78*, 1396.
41. Li, R.; Shen, J.; Tian, F. A theoretical study of the thermodynamic properties of $YMgX_4$ (*X*= Co, Ni, Cu) compounds. *AIP Advances* **2014,** *4*, 097123.
42. Wang, J.-W.; Yang, F.; Fan, T.-W.; Tang, B.-Y.; Peng, L.-M.; Ding, W.-J. Theoretical investigation of new type of ternary magnesium alloys $AMgNi_4$ (*A* = Y, La, Ce, Pr and Nd). *Physica B* **2011,** *406*, 1330–1335.
43. Wang, N., Zhang, W.; Tang, B.; Gao, H.-T.; He, E.; Wang, L. Structural, elastic and electronic properties of typical $NdMgT_4$ (*T* = Co, Ni, Cu) alloys from *ab* initio calculation. *Physica B: Condensed Matter* **2018,** *540*, 38–42.

Fig. 1. Change of the unit cell volume with Co content for $TbMgNi_{4-x}Co_x$ (x = 0–4) compounds.

Fig. 2. Hydrogenation properties of the $TbMgNi_{4-x}Co_x$ alloys: hydrogen absorption isotherms at 25 °C (*a*); evolution of the equilibrium pressure with x(Co) (*b*), comparison of *PCT* curves for the $TbMgCo_4$–H_2 system at 25 and 50°C (*c*), and first hydrogenation curves for the $TbMgNi_{4-x}Co_x$ (*d*).

Fig. 3. XRD patterns of the selected $TbMgNi_{4-x}Co_x$ hydrides (*a*,*b*) and evolution of the cell parameters versus Co content (*c*,*d*).

Fig. 4. Refined NPD pattern (1 – 97 wt.% $TbMgCo_4D_6$, 2 – 3 wt.% MgO) and unit cell projection of the $TbMgCo_4D_6$ deuteride with an environment of D atoms around Co and Mg.

Fig. 5. Density of states of $TbMgNi_{4-x}Co_x$ compounds and $TbMgNi_{4-x}Co_xH_6$ hydrides for x = 0, 2, 4. Red area corresponds to the total contribution whereas yellow and green areas correspond to the Ni and Co parts respectively. The Fermi level has been chosen as the origin of energy.